CHINESE OPTICS LETTERS

Vol. 22, No. 4 | April 2024

Second-harmonic generation in periodic fork-shaped $\chi^{(2)}$ gratings at oblique incidence

Yan Sheng (盛 艳)[1,2*], Shan Liu (刘 山)[3**], Xiaokang Hu (胡效康)[1,2], Xin Chen (陈 鑫)[4], Tianxiang Xu (徐天翔)[1,2], Ruwei Zhao (赵如薇)[1,2], and Wieslaw Krolikowski[3]

[1] Laboratory of Infrared Materials and Devices, Research Institute of Advanced Technologies, Ningbo University, Ningbo 315211, China

[2] Engineering Research Center for Advanced Infrared Photoelectric Materials and Devices of Zhejiang Province, Ningbo University, Ningbo 315211, China

[3] Department of Quantum Science and Technology, Research School of Physics, Australian National University, Canberra ACT 2601, Australia

[4] School of Physics and Optoelectronics Engineering, Xidian University, Xi'an 710071, China

*Corresponding author: shengyan@nbu.edu.cn

**Corresponding author: shanliu@anu.edu.au

Received November 30, 2023 | Accepted January 11, 2024 | Posted Online April 25, 2024

Three-dimensional (3D) nonlinear photonic crystals have received intensive interest as an ideal platform to study nonlinear wave interactions and explore their applications. Periodic fork-shaped gratings are extremely important in this context because they are capable of generating second-harmonic vortex beams from a fundamental Gaussian wave, which has versatile applications in optical trapping and materials engineering. However, previous studies mainly focused on the normal incidence of the fundamental Gaussian beam, resulting in symmetric emissions of the second-harmonic vortices. Here we present an experimental study on second-harmonic vortex generation in periodic fork-shaped gratings at oblique incidence, in comparison with the case of normal incidence. More quasi-phase-matching resonant wavelengths have been observed at oblique incidence, and the second-harmonic emissions become asymmetric against the incident beam. These results agree well with theoretic explanations. The oblique incidence of the fundamental wave is also used for the generation of second-harmonic Bessel beams with uniform azimuthal intensity distributions. Our study is important for a deeper understanding of nonlinear interactions in a 3D periodic medium. It also paves the way toward achieving high-quality structured beams at new frequencies, which is important for manipulation of the orbital angular momentum of light.

Keywords: second-harmonic generation; nonlinear photonic crystal; periodically poled ferroelectric crystal; quasi-phase matching; nonlinear wavefront shaping.

DOI: 10.3788/COL202422.041902

1. Introduction

Second-harmonic generation (SHG) has been intensively studied as a fundamental process to discover principles of light interactions with nonlinear optical systems. It also has important applications in laser sources, optical imaging, and engineering[1–3]. Phase matching is an essential condition to achieve efficient SHG. For this purpose, quasi-phase matching (QPM) was proposed in the 1960s to synchronize the phase velocities of optical waves employing spatial modulations of the second-order nonlinear coefficient $\chi^{(2)}$[4–8]. Periodic modulation of $\chi^{(2)}$ provides in a Fourier space a set of reciprocal lattice vectors to compensate for the phase mismatch of the SHG process, i.e., $k_2 - 2k_1 - G = 0$, where k_1 and k_2 are wave vectors of the fundamental and second-harmonic (SH) waves, respectively, and G is a reciprocal lattice vector.

The spatial modulation of the second-order nonlinearity $\chi^{(2)}$ can be realized through ferroelectric domain engineering[9,10]. Using the traditional electric field poling technique, various ferroelectric domain patterns with one- or two-dimensional $\chi^{(2)}$ modulation have been fabricated[6,11–13]. Analogous to the photonic crystals with spatially modulated dielectric constant in linear optics, these microstructures with spatially modulated second-order nonlinearity were called nonlinear photonic crystals (NPCs)[5]. Very recently, to fabricate 3D NPCs the optical poling with near-infrared laser pulses has been demonstrated[14,15]. The illumination of tightly focused infrared pulses introduces a great temperature gradient and then a thermal electric field to invert ferroelectric domains inside the focal volume of the light beam. Three-dimensionally scanning the laser focus inside transparent ferroelectric crystals, 3D NPCs were fabricated[16–18].

© 2024 Chinese Optics Letters

Inspired by the invention of femtosecond laser poling that enables precise domain engineering in three dimensions, employing 3D NPCs for nonlinear wavefront shaping has attracted great interest recently[19–21]. In this process, frequency conversion and beam-shaping functions are simultaneously realized in a single piece of nonlinear optical crystal. So far, optical second-harmonic vortices and higher-order Hermite–Gaussian beams have been generated in simple laser-induced domain structures[22–25]. Among these structures, periodic fork-shaped $\chi^{(2)}$ gratings are commonly used for SH vortex beam generation[20]. The fork-shaped $\chi^{(2)}$ distribution allows conversion of a fundamental Gaussian beam to a second vortex harmonic with spiral phase front, and the periodicity of the $\chi^{(2)}$ forks ensures efficient interaction via quasi-phase matching. The second harmonic vortex beams are important because shorter wavelengths usually yield higher resolution in optical trapping and materials engineering applications.

However, the previous studies on the SH vortex beam generation in periodic fork-shaped $\chi^{(2)}$ gratings have been restricted to normal incidence of the fundamental beam, i.e., the fundamental wave propagates perpendicularly to the fork periodicity[20]. Accordingly, the SH vortex beams were generated symmetrically against the fork structures, and the involved phase-matching conditions were easy to understand. In this work, we present an experimental study on the SH vortex beam generation at oblique incidence of the fundamental Gaussian wave. Compared with the case of normal incidence, the SH emission becomes asymmetric with respective to the fork structure, and more resonant wavelengths are observed. We also show the donut-like SH vortices are obtained only at these resonant wavelengths when the QPM condition is perfectly fulfilled. Our study is useful for deeper understanding of nonlinear wave interactions in 3D photonic structures. The oblique incidence also offers a promising way to achieve perfectly phase-matched SH Bessel beams with large conical angles, which is important to applications in optical trapping.

2. Sample Fabrication

To fabricate the periodic fork-shaped NPC, the femtosecond laser poling technique was used. The infrared pulses were tightly focused into a z-cut $Ca_{0.28}Ba_{0.72}Nb_2O_6$ (CBN) crystal to invert ferroelectric domains in the focal volume of the pulses[26]. The sizes of the CBN crystal are 5 mm × 5 mm × 0.5 mm in length (x), width (y), and thickness (z), respectively. The crystal was mounted on a translational stage that can be accurately positioned in three orthogonal directions. The infrared pulses (150 fs, 800 nm, Mira Coherent) were focused using an objective lens (NA = 0.65, 50×, Olympus LCPLN50XIR) and incident normally to the z surface of the crystal [Fig. 1(a)]. The focal size was estimated around 1 μm. The first layer of the fork structures was created at a depth of 136.92 μm below the crystal surface. In this process, the writing laser beam was focused at the depth of 136.92 μm below the surface, and then, the sample was translated against the writing beam for 5 μm to induce ferroelectric domain inversion in the focus. After that, the laser beam was blocked by an automatic shutter and the sample moved to the next region of domain inversion. The distance between the neighboring positions was selected to be 1 μm, which is short enough to ensure the merge of neighboring domains to form a smooth line or curve of inverted domain. After the writing of the first layer, the laser beam was blocked by the automatic shutter again, and the sample moved to the next layer of domain inversion, which was 22.82 μm above the first layer, i.e., the period of the fork grating was 22.82 μm. This period is designed to phase match the SHG at the fundamental wavelength of 1275 nm using the reciprocal lattice vector G_{012}[27]. Repeating the procedures above, we fabricated six-layer fork-shaped gratings along the depth (z axis) of the crystal.

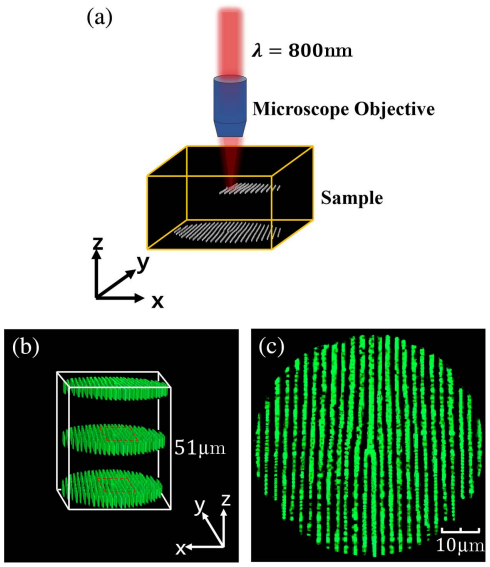

Fig. 1. (a) Illustrating the femtosecond laser writing of periodic fork-shaped $\chi^{(2)}$ gratings in a z-cut CBN crystal; (b) 3D image of the fabricated periodic fork domain structures, obtained using Čerenkov SH microscopy[28]; (c) Čerenkov microscopic image of a single layer of the structure.

The fabricated domain structures were imaged using Čerenkov SH microscopy[28], with three layers of domains being displayed in Fig. 1(b). The Čerenkov SH microscopy works on the stronger Čerenkov SH signal at ferroelectric domain walls owing to the abrupt change of the second-order nonlinear coefficient $\chi^{(2)}$ across the domain wall[29]. The Čerenkov SH microscopic image of one of the domain layers is shown in Fig. 1(c) for more structural details.

3. SH Experiment

The SHG experiment was conducted in the infrared spectral range. The fundamental beam came from a mode-locked Ti:sapphire femtosecond laser oscillator (Chameleon Optical Parametric Oscillator, Coherent) with tunable wavelengths in the range of 680–1600 nm. The pulse width is 8 fs and the repetition rate is 80 MHz. The average power of the fundamental

beam was controlled by the combination of a half-wave plate and a polarizer. The beam was linearly polarized along the x axis of the crystal, focused by a microscope objective (NA = 0.1), and incident from the z surface of the crystal. The crystal was mounted on a rotational stage such that the incident angle of the fundamental beam was adjustable. The SHG at normal (incident angle $\alpha = 0°$) and oblique incidence ($\alpha = 1.27°$) was experimentally detected, respectively. The SH emission was projected onto a far-field screen and recorded by a CCD camera, with the fundamental beam being filtered out with a short-pass filter.

4. Results and Discussions

4.1. SHG at normal incidence

The SHG at normal incidence of the fundamental beam was studied first as a reference. Figure 2(a) shows the wavelength tuning response of the SH in this case, namely, the variation of the power of the SH with the wavelength of incident light, where the resonances correspond to quasi-phase-matching interactions using different orders of reciprocal lattice vectors. The recorded far-field SH images at each quasi-phase-matching wavelength are displayed in Figs. 2(b). It is seen that the SH signals are generated noncollinearly with the fundamental beam (marked by the red circle in the figures), exhibiting symmetric intensity distributions against the fundamental beam. According to our analysis, the emission resonances observed at 1270, 1160, and 1070 nm are corresponding to the nonlinear Bragg diffraction with participations of reciprocal lattice vectors $G_{0,\pm1,2}$, $G_{0,\pm1,3}$, and $G_{0,\pm1,4}$, respectively. These wavelengths agree well with the calculated values of 1269, 1147, and 1065 nm, respectively. The phase-matching diagrams are illustrated in the Fig. 2(c). In fact, the transverse phase-matching conditions are the same for these three wavelengths, which can be written as $k_2 \sin\theta_2 = G_{0,\pm1,0}$, where $G_{0,\pm1,0} = 2\pi/\Lambda_y$, with $\Lambda_y = 2.3\,\mu m$ being the transverse period of the grating structure. The longitudinal phase-matching conditions are satisfied using different reciprocal lattice vectors, i.e., $k_2 \cos\theta_2 = 2k_1 + mG_{0,0,1}$, where $G_{0,0,1} = 2\pi/\Lambda_z$, $\Lambda_z = 22.82\,\mu m$ is the longitudinal period, and m is an integer denoting the order of longitudinal QPM interactions. For the SHG at 1270, 1160, and 1070 nm, m takes the values of 2, 3, and 4, respectively. The slight differences between the experimental and calculated wavelengths may come from the imperfection of the fabricated periodic grating structures. It is known that structural errors are unavoidable in any poling process, which can lead to wavelength shift of QPM resonance. Moreover, the refractive indices used in the calculations may not be accurate enough[27].

It should be noted that the SH signals are also observable at nonresonant wavelengths, but the donut-shaped SH vortices can be obtained only at those resonant wavelengths, when the quasi-phase-matching condition is fully satisfied.

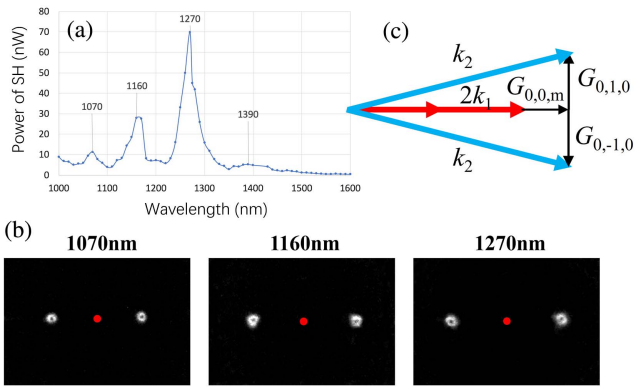

Fig. 2. (a) Wavelength tuning response of the SHG in periodic fork-shaped grating at normal incidence; (b) recorded SH images at resonant wavelengths of 1270, 1160, and 1070 nm in the far field. They correspond to QPM interactions involving different orders of longitudinal reciprocal lattice vectors. (c) The phase-matching diagrams at these resonance wavelengths; the transverse phase-matching conditions are the same for these three wavelengths, but the longitudinal conditions are different. From left to right (1070 to 1270 nm), the corresponding reciprocal lattice vectors in the longitudinal direction are $G_{0,0,4}$, $G_{0,0,3}$, $G_{0,0,2}$, i.e., m = 4, 3, 2, respectively.

4.2. SHG at oblique incidence

The SHG at oblique incidence was studied at an incident angle of 1.27°. This angle was selected just as a representative. We first analyze the phase-matching conditions in this case, with the SHG using $G_{0,\pm1,2}$ being studied as an example. As shown in Figs. 3(a) and 3(b), the QPM interaction using $G_{0,-1,2}$ fulfills the conditions,

$$k_2 \sin\theta_2 - 2k_1 \sin\theta_1 = G_{0,1,0}, \tag{1}$$

$$k_2 \cos\theta_2 - 2k_1 \cos\theta_1 = G_{0,0,2} = 2G_{0,0,1}, \tag{2}$$

while the process using $G_{0,1,2}$ satisfies

$$k_2' \sin\theta_2 + 2k_1' \sin\theta_1 = G_{0,1,0}, \tag{3}$$

$$k_2' \cos\theta_2 - 2k_1' \cos\theta_1 = G_{0,0,2} = 2G_{0,0,1}. \tag{4}$$

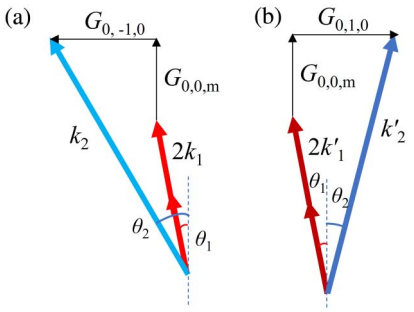

Fig. 3. (a) and (b) Quasi-phase-matching diagrams of SHGs using reciprocal lattice vectors $G_{0,1,2}$ and $G_{0,-1,2}$ at oblique incidence of the fundamental wave, respectively. These two conditions are usually fulfilled at different wavelengths.

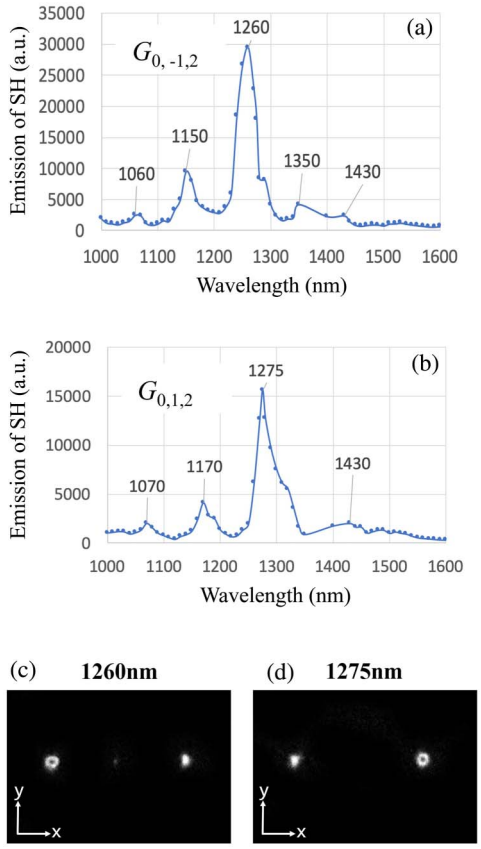

Fig. 4. (a) and (b) Experimental wavelength tuning responses of the SHs using $G_{0,-1,2}$ and $G_{0,1,2}$, respectively; (c) and (d) recorded SH images at fundamental wavelengths of 1260 and 1275 nm, respectively.

In fact, these two sets of equations are usually satisfied at different wavelengths; as verified by the experimental results shown in Figs. 4(a) and 4(b), the observed SH beams generated via $G_{0,1,2}$ and $G_{0,-1,2}$ exhibited different wavelength tuning responses, with their resonant wavelengths being blue- (1260 nm) or red-shifted (1275 nm) against that at normal incidence (1270 nm), respectively. These agree well with the calculated wavelengths of 1255 and 1285 nm, respectively. The slight difference between the experiment and theory mainly comes from the imperfection of the experimental ferroelectric domain structures, since the random structure errors are unavoidable in any poling processes.

4.3. Application of oblique incidence to Bessel beam SH generation

The Bessel beam has received great interest recently because it does not diffract with its propagation, which is extremely useful for many applications such as optical trapping and particle manipulation. Figure 5(a) shows a typical kind of ferroelectric domain structures that is capable of converting a fundamental Gaussian beam into an SH Bessel beam; Fig. 5(b) shows its Fourier transform spectrum. In the case of normal incidence, the SH emission is noncollinear, and the k_2 sphere intersects

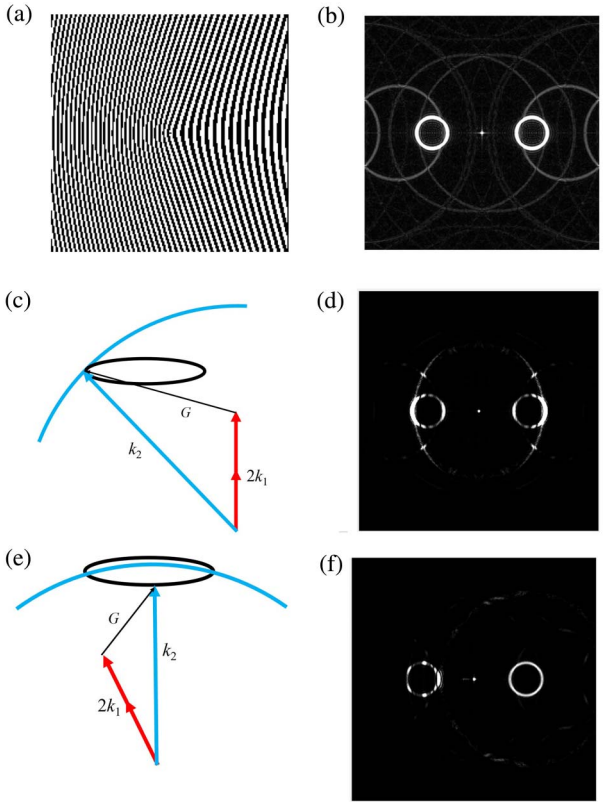

Fig. 5. (a) Ferroelectric domain structure for conversion of a fundamental Gaussian beam into an SH Bessel beam; (b) Fourier transform spectrum of this structure; (c) phase-matching conditions are different along the azimuthal directions at normal incidence of the fundamental Gaussian beam. Here an extreme case is given where phase-matching conditions are obtained only on the left edge of the ring-shaped reciprocal vectors. (d) Calculated SHs at normal incidence; (e) the phase-matching conditions become the same for all the azimuthal angles by employing an obliquely incident fundamental beam. (f) Calculated SH Bessel beams at the oblique incidence.

with the reciprocal ring only at partial areas. For example, Fig. 5(c) shows an extreme case where the perfect phase-matching condition can only be obtained along the edge of the reciprocal ring. Accordingly, the SH Bessel beams exhibit spatially varied azimuthal intensity, as shown in Fig. 5(d). This effect is not obvious when the conical angle is rather small in experiment. However, measures must be taken for larger conical emission angles, since uneven intensity distributions may destroy all applications of Bessel beams.

Here we propose a solution to this problem by utilizing the oblique incidence of the fundamental Gaussian beam. The principle is to steer one of the SH emissions perpendicular to the reciprocal ring, such that the phase-matching conditions are the same for all emission angles, as shown in Fig. 5(e). In this case, the SH Bessel beam calculated with the Fourier transform method is shown in Fig. 5(f). As predicted, the Bessel beam at the right side presents a uniform azimuthal intensity distribution. This property is important for applications of Bessel beam to optical tweezering and particle trapping.

5. Conclusion

In summary, we have fabricated periodic fork-shaped $\chi^{(2)}$ gratings using the optical poling of ferroelectric domains in a z-cut CBN crystal. The SHG is experimentally studied at normal and oblique incidences, respectively. It is shown that more spectral resonances are obtained at the oblique incidence. The experimental results agree well with calculations. We also propose the oblique incidence of fundamental beam can be used for the generation of an SH Bessel beam with uniform intensities, which is important for optical tweezering and particle trapping. Our studies were conducted with the SH vortex and Bessel beams as examples. The same concepts and methods apply to many other nonlinear optical processes such as cascaded third-harmonic generation with predesigned phase and amplitude properties.

Acknowledgements

This work was supported by the National Natural Science Foundation of China (Nos. 12274248, 62275136, 61905124, and 61905125), the Natural Science Foundation of Zhejiang Province (No. LY22F050009), the Australian Research Council, and the K. C. Wong Magna Fund of Ningbo University.

References

1. P. Campagnola, "Second harmonic generation imaging microscopy: applications to diseases diagnostics," Anal. Chem. **83**, 3224 (2011).
2. B. Kraus, F. Dawel, S. Hannig, *et al.*, "Phase-stabilized UV light at 267 nm through twofold second harmonic generation," Opt. Express **30**, 44992 (2022).
3. Y. H. Ren, P. Maity, D. Ascienzo, *et al.*, "Second harmonic generation studies of interfacial strain engineering in $BaZr_{0.2}Ti_{0.8}O_3$," Adv. Electron. Mater. **9**, 2300497 (2023).
4. J. A. Armstrong, N. Bloembergen, J. Ducuing, *et al.*, "Interactions between light waves in a nonlinear dielectric," Phys. Rev. **127**, 1918 (1962).
5. V. Berger, "Nonlinear photonic crystals," Phys. Rev. Lett. **81**, 4136 (1998).
6. N. G. R. Broderick, G. W. Ross, H. L. Offerhaus, *et al.*, "Hexagonally poled lithium niobate: a two-dimensional nonlinear photonic crystal," Phys. Rev. Lett. **84**, 4345 (2000).
7. S. M. Saltiel, D. N. Neshev, R. Fischer, *et al.*, "Generation of second-harmonic conical waves via nonlinear Bragg diffraction," Phys. Rev. Lett. **100**, 4 (2008).
8. Y. Zhang, Y. Sheng, S. N. Zhu, *et al.*, "Nonlinear photonic crystals: from 2D to 3D," Optica **8**, 372 (2021).
9. X. Q. Yu, P. Xu, Z. D. Xie, *et al.*, "Transforming spatial entanglement using a domain-engineering technique," Phys. Rev. Lett. **101**, 233601 (2008).
10. G. Rosenman and A. Skliar, "Domain engineering for nonlinear optical devices," Ferroelectrics **221**, 129 (1999).
11. C. Canalias and V. Pasiskevicius, "Mirrorless optical parametric oscillator," Nat. Photonics **1**, 459 (2007).
12. Y. Sheng, J. Dou, B. Ma, *et al.*, "Broadband efficient second harmonic generation in media with a short-range order," Appl. Phys. Lett. **91**, 011101 (2007).
13. N. V. Bloch, K. Shemer, A. Shapira, *et al.*, "Twisting light by nonlinear photonic crystals," Phys. Rev. Lett. **108**, 233902 (2012).
14. X. Chen, P. Karpinski, V. Shvedov, *et al.*, "Ferroelectric domain engineering by focused infrared femtosecond pulses," Appl. Phys. Lett. **107**, 141102 (2015).
15. J. Thomas, V. Hilbert, R. Geiss, *et al.*, "Quasi phase matching in femtosecond pulse volume structured x-cut lithium niobate," Laser Photonics Rev. **7**, L17 (2013).
16. T. X. Xu, K. Switkowski, X. Chen, *et al.*, "Three-dimensional nonlinear photonic crystal in ferroelectric barium calcium titanate," Nat. Photonics **12**, 591 (2018).
17. D. Z. Wei, C. W. Wang, H. J. Wang, *et al.*, "Experimental demonstration of a three-dimensional lithium niobate nonlinear photonic crystal," Nat. Photonics **12**, 596 (2018).
18. J. Imbrock, L. Wesemann, S. Kroesen, *et al.*, "Waveguide-integrated three-dimensional quasi-phase-matching structures," Optica **7**, 28 (2020).
19. S. Liu, K. Switkowski, C. L. Xu, *et al.*, "Nonlinear wavefront shaping with optically induced three-dimensional nonlinear photonic crystals," Nat. Commun. **10**, 3208 (2019).
20. D. Wei, C. Wang, X. Xu, *et al.*, "Efficient nonlinear beam shaping in three-dimensional lithium niobate nonlinear photonic crystals," Nat. Commun. **10**, 4193 (2019).
21. A. Karnieli, S. Tsesses, G. Bartal, *et al.*, "Emulating spin transport with nonlinear optics, from high-order skyrmions to the topological Hall effect," Nat. Commun. **12**, 1092 (2021).
22. N. N. Wang, S. Liu, T. X. Xu, *et al.*, "Structuring light beams via nonlinear diffraction in 3D nonlinear photonic crystal," Opt. Laser Technol. **168**, 109994 (2024).
23. B. Zhu, H. G. Liu, Y. A. Liu, *et al.*, "Second-harmonic computer-generated holographic imaging through monolithic lithium niobate crystal by femtosecond laser micromachining," Opt. Lett. **45**, 4132 (2020).
24. X. Hu, S. Liu, T. Xu, *et al.*, "Nonlinear generation of an optical bottle beam in domain-engineered ferroelectric crystals," Opt. Lett. **48**, 5527 (2023).
25. P. C. Chen, C. W. Wang, D. Z. Wei, *et al.*, "Quasi-phase-matching-division multiplexing holography in a three-dimensional nonlinear photonic crystal," Light Sci. Appl. **10**, 146 (2021).
26. X. Chen, P. Karpinski, V. Shvedov, *et al.*, "Ferroelectric domain engineering by focused infrared femtosecond pulses," Appl. Phys. Lett. **107**, 141102 (2015).
27. M. Esser, M. Burianek, P. Held, *et al.*, "Optical characterization and crystal structure of the novel bronze type $Ca_xBa_{1-x}Nb_2O_6$ (x = 0.28; CBN-28)," Cryst. Res. Technol. **38**, 457 (2003).
28. Y. Sheng, A. Best, H. J. Butt, *et al.*, "Three-dimensional ferroelectric domain visualization by Cerenkov-type second harmonic generation," Opt. Express **18**, 16539 (2010).
29. Y. Sheng, V. Roppo, K. Kalinowski, *et al.*, "Role of a localized modulation of $\chi^{(2)}$ in Čerenkov second-harmonic generation in nonlinear bulk medium," Opt. Lett. **37**, 3864 (2012).